Journal of Molecular Liquids 221 (2016) 26–32

Contents lists available at ScienceDirect

Journal of Molecular Liquids

journal homepage: www.elsevier.com/locate/molliq

Molecular dynamics investigation on structural and transport properties of Na_3AlF_6–Al_2O_3 molten salt

Xiaojun Lv [a], Zhenming Xu [a], Jie Li [a,*], Jiangan Chen [b], Qingsheng Liu [c]

[a] School of Metallurgy and Environment, Central South University, Changsha 410083, China
[b] Faculty of Resource and Environmental Engineering, Jiangxi University of Science and Technology, Ganzhou 341000, China
[c] Faculty of Metallurgical and Chemical Engineering, Jiangxi University of Science and Technology, Ganzhou 341000, China

ARTICLE INFO

Article history:
Received 21 November 2015
Received in revised form 19 May 2016
Accepted 21 May 2016
Available online 25 May 2016

Keywords:
Molecular dynamics
Structure properties
Transport properties
Na_3AlF_6–Al_2O_3
Molten salt

ABSTRACT

To study the effect of Al_2O_3 concentration on the local structure and transport properties of Na_3AlF_6–Al_2O_3 molten salt, molecular dynamics (MD) simulations with the Coulomb–Buckingham potential model were carried out. MD simulation results show $[AlF_4]^-$, $[AlF_5]^{2-}$ and $[AlF_6]^{3-}$ groups coexist in Na_3AlF_6–Al_2O_3 molten salt and $[AlF_6]^{3-}$ ions are the dominant species at low Al_2O_3 concentration of 1–2 wt%. The percentages of $[AlF_4]^-$, $[AlF_5]^{2-}$ and $[AlF_6]^{3-}$ groups are approximately equal at 3 wt% Al_2O_3 and $[AlF_4]^-$ ions become the major species at 4 wt% Al_2O_3. O atoms mainly exist in the form of bridge O_b up to 90%, worsening the fluidity and transport properties of Na_3AlF_6–Al_2O_3 molten salt. According to quantum chemical calculations, Al—F and Al—O bonds in the $[Al_2OF_6]^{2-}$ groups have ionic characters as well as partial covalent characters due to the hybridization of F, O-2p and Al-3s (3p) orbitals, while Na—F and F—F bonds are ionic. The orders of particle's diffusion ability follow as $Na^+ > F^- > Al^{3+} > O^{2-}$. In addition, Al_2O_3 acts as bridges connecting ionic structure networks and more Al_2O_3 can increase the polymerization degree of the local structure in Na_3AlF_6–Al_2O_3 molten salt, and the viscosity increase and ionic conductivity reduce accordingly.

1. Introduction

Understanding the structure and transport properties of $[AlF_x]^{3-x}$ and aluminum-fluorine-oxygen groups of Na_3AlF_6–Al_2O_3 molten salt has become an interesting issue, because they play key roles in the molten salt physical and chemical properties of the industrial Hall–Heroult process for electro-deposition of Al metal from alumina [1–3]. In addition, a better knowledge of the microscopic structure and transport properties of Na_3AlF_6–Al_2O_3 molten salt is required for the correct interpretation of their spectroscopic data. For this reason, Na_3AlF_6 molten salt has been already studied extensively both in theoretical calculations [4–7] and experiments [8–11]. Gilbert and coworkers have reproduced the structure properties and Raman spectra of several NaF–AlF_3 crystal compounds by using the molecular dynamics (MD) simulation based on the rigid ionic (RI) model, and proposed that, only tetrahedral $[AlF_4]^-$ ions exist in the melts of $NaAlF_4$ [10]. In 2014, S. Cikit et al. pointed out five-coordinated $[AlF_5]^{2-}$ and six-coordinated $[AlF_6]^{3-}$ ions are the dominant groups in Na_3AlF_6 molten salt (cryolite) by MD simulation [6]. Furthermore, high temperature Raman [9,12] and NMR [13] experiment give an alternative experimental window to insight the evolution of $[AlF_x]^{3-x}$ groups with different molten salt compositions. The predominance of $[AlF_5]^{2-}$ in cryolite molten salt, proposed by S. Cikit is consistent with the NMR data [8]. Above researches mainly focused on the binary NaF–AlF_3 molten salt, while in the practical industrial production of aluminum electrolysis, 1–4 wt% Al_2O_3 as solute are added to NaF–AlF_3 molten salt. The solute Al_2O_3 can produce a great impact on the partial structure and transport properties of Na_3AlF_6 molten salt, in spite of its low quantity [14].

For Na_3AlF_6–Al_2O_3 molten salt, V. Lacassagne et al. have studied the structure of high-temperature Na_3AlF_6–Al_2O_3 molten salt by multinuclear NMR [13,15,16]. However, experimental measurements on molten fluoride salts can be limited by the expensive cost and strong corrosion of fluoride salts. Fortunately, computational simulation assisted with experiment provide a low cost and powerful method to explore the molten fluoride salts [17]. With respect to the ab initio method, MD simulation can provide more useful information such as dynamical and transport properties. In addition, ab initio is very computationally intensive and therefore limited to much smaller system with shorter simulation time than classical MD simulation [17,18]. However, MD simulation of Na_3AlF_6–Al_2O_3 molten salt is rarely seen. So far, only D.K. Belashchenko et al. have studied on the structure, thermodynamic, and electrical transport properties of Na_3AlF_6–Al_2O_3 molten salt by classical MD simulation [14]. The MD simulation method in D.K. Belashchenko's work doesn't contain the dipole-dipole attractive interaction between two atoms (equivalent to Born–Mayer potential model)

* Corresponding author.
E-mail address: 15216105346@163.com (J. Li).

http://dx.doi.org/10.1016/j.molliq.2016.05.064
0167-7322/

and only consider the coulomb and short-range repulsive interactions. The overlook of dipole-dipole attractive interaction may reduce the accuracy of describing the short-range structure of Na_3AlF_6–Al_2O_3 molten salt. Apart from the Born–Mayer potential model, Coulomb–Buckingham potential model allows a straightforward treatment of the dipole-dipole attractive interaction of atoms, which has been successfully applied in the fields of MD simulation of glass [19–21]. It can improve the accuracy of reproducing the short and medium-range structure of Na_3AlF_6–Al_2O_3 molten salt.

In this work, the multi-scale simulation with molecular dynamics by the Coulomb–Buckingham potential model [22,23] and ab initio method were carried out to enhance our knowledge of local structure and transport properties of Na_3AlF_6–Al_2O_3 molten salt. The effect of Al_2O_3 concentration on basic structure-transport properties were calculated and compared to the experimental measurements to verify the Coulomb-Buckingham potential model and parameters of Na_3AlF_6–Al_2O_3 molten salt.

2. Computational methods

2.1. Force field potential

A key of molecular dynamics simulation is to choose an appropriate potential function with corresponding parameters which are suitable for calculation of particle interactions. In the two-body potential model [22,23], there are three kinds of potential function: long-range coulomb interaction, short-range repulsion interaction and van der Waals (vdW) force. It has been generally and successfully used in MD simulation of glass and ionic melt, and it was applied here:

$$V_{LR}^{ij}(r_{ij}) = \frac{q_i q_j}{4\pi\varepsilon_0}\frac{1}{r_{ij}} \tag{1}$$

$$V_{SR}^{ij}(r_{ij}) = A_{ij}\exp(-\beta_{ij} r_{ij}) - \frac{C_{ij}}{r_{ij}^6} \tag{2}$$

where, the long-range potential, $V_{LR}^{ij}(r_{ij})$, in Eq. (1) describes the coulomb interaction, which is defined for the interactions between two atoms, i and j. Here, q_i, ε_0 and r_{ij} donate the charge of ions, the dielectric constant in vacuum, and the distance between two particles, respectively. The short-range potential, $V_{SR}^{ij}(r_{ij})$, in Eq. (2) works between the cation–cation, cation–anion and anion–anion pairs. We selected the Buckingham potential for the short-range potential, and A_{ij},β_{ij}, and C_{ij} are the potential parameters that determine the pair interactions between two particles.

Coulomb interaction acts between all species whereas the Buckingham potential acts for the Na—F, Al—F, Al—Al, Na—Al, F—F, Na—O, Al—O and F—O short-range interactions. The charge of ions as this: Na = 0.72e, Al = 2.16e, O = −1.44e, F = −0.72e, which were obtained from our previous DFT calculation for a Na_3AlF_6 crystal cell. Table 1 lists all force field parameters used in this work. It is worth highlighting that, for the first time, a set of Buckingham parameters A_{ij},β_{ij}, and C_{ij} for all atom pairs were fitted by ourselves through scanning the potential energy curve of atom pairs with the ab initio method.

To test the validation of interatomic potential parameters, the lattice parameters of NaF, AlF_3, Na_3AlF_6 and Al_2O_3 crystals were reproduced and compared to the theoretical and experimental results [24,25], as shown in Table 2. As a whole, the lattice parameters of above crystal reproduced by the Buckingham potential parameters are in good agreement with the theoretical and experimental results, whereas some deviations for AlF_3 crystal can be observed. It is important to emphasize that the portability and accuracy of potential in itself is a pair of contradictory, the Al—Al pair potential is difficult to reproduce well the lattice parameters of AlF_3, Na_3AlF_6 and Al_2O_3 crystals simultaneously. Considering our goal mainly focusing on the clusters of Al—F and Al–F–O, so the inaccuracy of Al—Al pair potential needs a bit of a respite.

Table 1
Buckingham interatomic potential parameters of Na_3AlF_6–Al_2O_3 molten salt.

Ions pair	A_{ij}[eV]	β_{ij}[Å]	C_{ij}[eV·Å^6]
Na–Na	0	1	0
Na–F	12230.42	4.28	90.89
Al–Al	9830.5	2.06	675
Na–Al	4929.05	3.22	0
Al–F	47181.82	5.48	22.75
F–F	24300.26	5.04	6.56
Na–O	9940.63	2.87	20.24
Al–O	3596.93	4.03	0
F–O	25230.57	7.88	4.32
O–O	435.63	2.57	0.49

2.2. Details of MD simulation

The DL-POLY package was employed for our MD simulations. The Verlet Leap-Frog algorithm was used with a time step of 1 fs to solve the equation of Newton motions [26]. Ewald sum was used for all Coulomb and multipolar interactions with a buffer width 0.5 Å and an accuracy of 10^{-5} kcal/mol. The short-range interaction cutoff was set to 15 Å [27,28]. Periodic boundary conditions were applied on all sides of those model boxes to create infinite systems with no boundaries, so that the calculated results would be more convincible. Initial configurations of 4000 ions for molecular dynamics were prepared by packing ions randomly in the simulation boxes in order to properly simulate the liquid state. The number of atoms of each molar compositions in the simulation box are shown in Table 3. To mix the system completely and eliminate the effect of the initial distributions, the simulation box systems were heated up to 4000 K in an NPT ensemble for 300 ps at 1.01 MPa, which means these simulations were run keeping the number of particles (N), pressure (P) and the temperature (T) of the simulation box systems as constants. Then these hot liquids were cooled down at a rate of 1 K/ps to the melting point of 1273 K. Another 200 ps of equilibriums at NPT ensemble were performed for relaxation. After these runs, convergences were achieved and the density differences between the initial and final state were less than 1%. Finally, the trajectories of atoms were collected for the following statistical calculation of structural and transport properties.

2.3. Statistics of structure information

The partial radial distribution function (PRDF) analysis was conducted from the MD trajectory to study the local structure of fluoride molten salt. The RDFs give the probability of finding an ion within a distance of Δr from a specified particle at the location of r and CNs show the average coordination number (CN) for atom i around atom j [29]. The equation of PRDF is expressed as below (Eq. (3)).

$$\mathrm{gij(r)} = \frac{V}{N_i N_j}\sum\nolimits_j \frac{\langle n_{ij}(r,\Delta r)\rangle}{4\pi r^2} \tag{3}$$

where, V is the volume of the MD box cell and N is the number of particle. N_{ij} $(r, \Delta r)$ is the average number of atom j surrounding a central atom i within a defined cut-off distance of Δr.

The first-shell coordination number (CN) of Al with the surrounding F anion was estimated by numerical integration of the PRDFs within a cut-off radius, which corresponds to the first minima of the corresponding partial $g_{\mathrm{Al\text{-}F}}(r)$ [27]. We referred to the integral of the PRDF as following function (Eq. (4)),

$$N_{\mathrm{Al\text{-}F}} = 4\pi\rho_F \int_0^R r^2 g_{\mathrm{Al-F}}(r)dr \tag{4}$$

Table 2
Comparison of our calculated and experimental lattice parameters for NaF, AlF_3, Na_3AlF_6 and Al_2O_3 crystals.

Species	Crystal structure	Space group	a(Å)	b(Å)	c(Å)
NaF	Cubic	Fm3m	4.69(4.71[a])	4.69 (4.71[a])	4.69 (4.71[a])
AlF_3	Rhombohedral	R3c	4.55(5.15[b])	4.55(5.15[b])	6.97(6.31[b])
Na_3AlF_6	Orthorhombic	*Immm*	5.57(5.4[c])	5.67(5.58[c])	7.98(7.76[c])
Al_2O_3	Rhombohedral	R3c	4.75(4.78[d], 4.76[d])	4.75(4.78[d], 4.76[d])	13.22(12.53[d], 12.99[d])

[a,b]Obtain by our first-principles calculation, [c]Reference [24], [d]Reference [25].

where, $g_{Al\text{-}F}(r)$ is the PRDF between species Al and F, and ρ_F the average number density of specie F.

As for the calculation of distribution of CN and F, O type, a MATLAB program was compiled to deal with the particle's trajectories of MD simulation.

2.4. Conditions of ab initio calculation

Calculations of density of states, electron density and Mulliken population of the selected molecular clusters were performed with the dispersion-corrected DFT-D method, provided by the CASTEP package. The generalized gradient approximation (GGA) with the Perdew–Burke–Ernzerhof (PBE) exchange correlation potential was used. Energy cutoff of 350 eV and a $1 \times 1 \times 1$ k-point mesh were chosen to in this quantum chemical calculation. The ultrasoft pseudo potentials (USPP) have been employed for all the ion-electron interactions. The ionic cores were represented by USPP for Na, Al and F atoms. The Na $2s^2 2p^6 3s^1$ electrons, Al $3s^2 3p^1$ electrons, F $2s^2 2p^5$ electrons and O $2s^2 2p^4$ were explicitly regarded as valence electrons.

2.5. Calculation of transport properties

Through statistical analysis of the particles' trajectories, the function of mean square displacement (MSD) vs time would be generated by the Einstein–Smoluchowshi equation [26].

$$\mathrm{MSD} = \left\langle \Delta \bar{r}(t)^2 \right\rangle = \frac{1}{N}\left\langle \sum \left| r_{i(t)} - r_{i(0)} \right| \right\rangle \tag{5}$$

where, $r_{i(t)}$ is the location of atom i at the time of t and the bracket means an ensemble average.

Combined with the knowledge of statistical thermodynamics, some transport properties of molten salt such as self-diffusion coefficient D, viscosity η and ionic conductivity σ would be calculated according to the MSD curves of particle. The relation between the self-diffusion coefficient D and the MSD curve is shown as below [30].

$$D = \lim_{t\to\infty} \frac{1}{6} \frac{d\left[\Delta r(t)^2\right]}{dt} \tag{6}$$

Then the viscosity η and ionic conductivity σ can be obtained by combining the self-diffusion coefficient D with the Einstein–Stokes formula [31] and Nernst–Einstein equation respectively [20].

$$\eta = \frac{K_B T}{2\pi D \lambda} \tag{7}$$

Table 3
Number of atoms of each molar compositions in the simulation box of Na_3AlF_6-Al_2O_3 molten salt, CR = 3.

wt%(Al_2O_3)	n(NaF)	n(AlF_3)	n(Al_2O_3)	Number of particle
1	1188	396	8	4000
2	1174	393	16	4000
3	1161	388	25	3999
4	1147	384	34	4000

$$\sigma = D\frac{nq^2}{K_B T} \tag{8}$$

where, K_B is the Boltzmann constant, which equals to 1.38×10^{-23} J/K, T is the temperature of the simulated molten salt, λ is the step length of ion diffusion and it is generally considered to be equal to the diameter of ion ($\lambda = 2R$), n presents the unit volume concentration of the carrier ion, and q is the charge of ion.

3. Results and discussions

3.1. Structure information

After MD simulation, the structure information was obtained from the statistical calculations of particle's trajectories. Fig. 1 shows a snapshot of ion structure states of Na_3AlF_6–Al_2O_3 molten salt (Al_2O_3 wt% = 4). The O^{2-} ions are shown in red, F^- in cyan, Al^{3+} in green, and Na^+ in blue. Gray lines represent bonds between Al, F and O when their distance are less than the first minimum in the radial distribution function. This snapshot indicates the ion structural characters are governed by the five-coordinated and six-coordinated Al species, corresponding to the trigonal bipyramid and octahedral symmetry. The O atom plays a role of bridge to connect two Al atoms to form the larger $Al_2OF_6^{2-}$ cluster structure.

3.1.1. Partial radial distribution functions and coordination number

The partial radial distribution functions (RDFs) of Na_3AlF_6–Al_2O_3 (Al_2O_3 wt% = 4) are shown in Fig. 2. It can be seen that for each ion pair, only several narrow peaks exist in the short-range, and RDF trend to a constant in the long-distance, and it means that though losing long-range order, there is still some tendency to keep the crystal local structure in the short-range. The first peaks of Al—F and Al—O are quite sharp, indicating these clusters are strong bonded in covalent

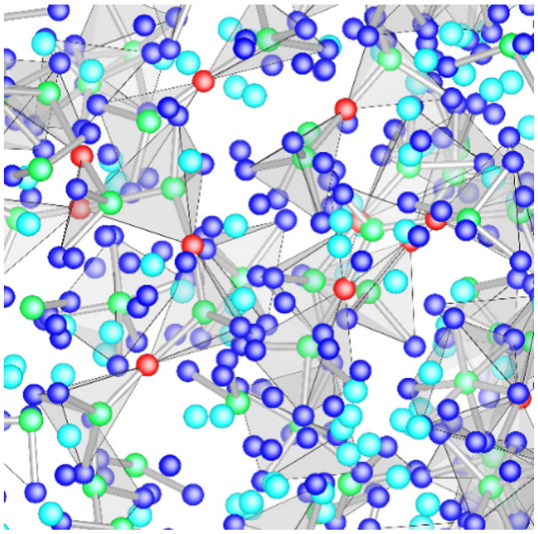

Fig. 1. Snapshot of the ion states in simulation of the Na_3AlF_6–Al_2O_3 (Al_2O_3 wt% = 4).

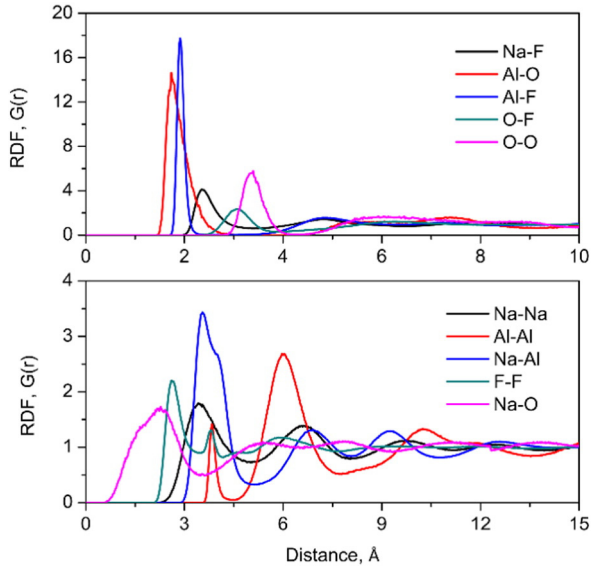

Fig. 2. Calculated partial radial distribution functions in Na_3AlF_6-Al_2O_3 molten salt, Al_2O_3 wt% = 4.

character. Table 4 summarizes the predicted structure characters for ion pairs of Na_3AlF_6–Al_2O_3 (Al_2O_3 wt% = 4) molten salt from our MD simulations in comparison with the previous calculated values from the literature [14]. With the integration of PRDF of Al—F and Al—O, average CN would be obtained and the ordinate value corresponding to the cutoff radius (first minimum of the PRDF) was considered to be the average CN. From Table 4, our calculated first-peak and first-minimum radius values are in good agreement with the previous calculated results. These first-peak radius located at 3.83–3.85 Å of Al—Al are twice larger than that of Al—F and Al—O, suggesting only a few Al—Al bonds are linked by the bridge F and O anions. As for a central Al^{3+}, F anions are located in its first shell, the second shells are Na^+ ions, and Al^{3+} ions reside in the third shell, implying that Coulomb forces dominate the interionic interactions of Na_3AlF_6–Al_2O_3 molten salt.

With the increase of Al_2O_3 concentration, the radius of first peak for all ion pairs increase accordingly, while the O—O decreases and O—F is an invariant value of 3.11 Å. For the first-minimum radius, it is observed that all the ions pairs increase except for O—F at a constant of 3.87 Å. When increasing the Al_2O_3 concentration, the first-shell average CN of Al—F decreases from 5.8 to 5.26, and Na—F decreases from 7.25 to 6.89. It indicates that adding more Al_2O_3 can induce the dissociation from $[AlF_6]^{3-}$ to $[AlF_4]^-$, $[AlF_5]^{2-}$.

3.1.2. Bond angles distributions

From Fig. 3a, the F–Al–F bond angles mainly distribute between 80° and 100°, while for 3 wt% and 4 wt% Al_2O_3, F–Al–F bond angles lie between 150° and 180°. The peak of F–Al–F bond angle is located at 86°, 86°, 84° and 167°, 80° and 165° respectively for 1–4 wt% Al_2O_3 of Na_3AlF_6–Al_2O_3 molten salt. The Al-O-Al bond angles mainly lie in the range of 160–180°, and the peak corresponds to 174°, 172°, 171° and 173°, respectively. It means that three atoms of Al–O–Al are close to a straight line and the Al–O–Al bond angle is determined by the covalent interaction between Al and O atom, not affected by the concentration of Al_2O_3. In sum, when increasing the percentage of Al_2O_3, ion structure of Na_3AlF_6–Al_2O_3 molten salt become loose, so the density of molten salt decrease accordingly.

3.1.3. F and O atom type

The distributions of CN were obtained by calculating the percentage of one Al ion having a given number of neighbors (F and O atoms) from all trajectories of MD simulations. Neighbors are these ions which are located inside the first shell corresponding to the radius of the RDF first-minimum illustrated in Fig. 2. Fig. 4a shows the percentage of Al^{3+} ions which are four-, five-, and six-coordinated in Na_3AlF_6–Al_2O_3 molten salt with different concentration of Al_2O_3. It is observed that the Al_2O_3 concentration of 2 wt% is the turning point of the curve. The $[AlF_4]^-$, $[AlF_5]^{2-}$ and $[AlF_6]^{3-}$ groups coexist in Na_3AlF_6–Al_2O_3 molten salt and the percentage of $[AlF_6]^{3-}$ ions decreases with the increase of concentration of Al_2O_3. In addition, $[AlF_6]^{3-}$ ions are the dominant species at low Al_2O_3 concentration of 1–2 wt%, corresponding to the octahedral symmetries and followed by $[AlF_5]^{2-}$ groups. Some $[AlF_4]^-$ and $[AlF_5]^{2-}$ ions can dissociate from the $[AlF_6]^{3-}$ groups at higher concentration of Al_2O_3. The percentages of $[AlF_4]^-$, $[AlF_5]^{2-}$ and $[AlF_6]^{3-}$ groups are approximately equal at 3 wt% Al_2O_3 and $[AlF_4]^-$ ions become the major species at 4 wt% Al_2O_3.

The F and O atom type (bridge F, O; non-bridge (terminal) F, O and freedom F, O) measures the structure polymerization degree of Na_3AlF_6–Al_2O_3 molten salt and has a greater impact on transport properties of molten salt. In Fig. 4b, it can be seen that, in Na_3AlF_6–Al_2O_3 system, the percentage of bridge F_b is small about 0.1–0.3% and the freedom F_f is up to 40–50%. This is consistent with the fact the first peak of Al—Al pair's PRDF located at 3.83–3.85 Å is twice larger than that of Al—F. With the Al_2O_3 concentration increasing from 2 wt% to 4 wt%, the proportion of freedom F_f decreases and the percentage of non-bridge F_{nb} increases, besides there is a small amplitude growth of bridge F_b.

The percentage of bridge O_b increases to 80% and non-bridge O_{nb}, freedom O_f decreases when Al_2O_3 concentration increasing from 2 wt% to 4 wt%. O atoms mainly exist in the form of the bridge O_b up to 90%, followed by the non-bridge O_{nb}, suggesting most O^{2-} anions

Table 4
Comparison of the first-peak, first-min radius (in brackets), first-shell average coordination number (CN) of ion pairs, F–Al–F average bond angle (in degree) and densities (in g/cm^3) of Na_3AlF_6–Al_2O_3 molten salt with other's calculated values.

	Ion pair	1 wt%	2 wt%	3 wt%	4 wt%	Ref. [14] (5 wt% Al_2O_3)
First-peak, min (in brackets) radius	Na–Na	3.47(4.79)	3.47(4.99)	3.45(5.01)	3.53(5.01)	3.53(first-peak)
	Al–Al	3.83(4.17)	3.83(4.23)	3.85(4.43)	3.85(4.53)	3.21
	Na–Al	3.57(5.17)	3.61(5.19)	3.61(5.27)	3.59(5.31)	3.59
	Na–F	2.41(3.45)	2.41(3.47)	2.39(3.53)	2.43(3.55)	2.41
	Al–F	1.89(2.73)	1.91(2.75)	1.91(2.81)	1.91(2.85)	1.82
	F–F	2.61(3.45)	2.67(3.47)	2.67(3.53)	2.71(3.55)	2.51
	Na–O	2.37(3.51)	2.37(3.57)	2.37(3.61)	2.41(3.63)	2.35
	Al–O	1.71(3.19)	1.77(3.31)	1.75(3.29)	1.73(3.31)	1.60
	O–F	3.11(3.87)	3.11(3.87)	3.11(3.87)	3.11(3.87)	2.69
	O–O	3.47(4.15)	3.39(4.51)	3.31(4.21)	3.37(4.32)	2.94
Average CN	Na–F	7.25	7.08	7.03	6.89	
	Al–F	5.8	5.74	5.4	5.26	5.71
Bond angle peak	F–Al–F	86	86	84, 167	80, 165	
	Al–O–Al	174	172	171	173	
Density		2.2	2.16	2.09	2.02	2.061

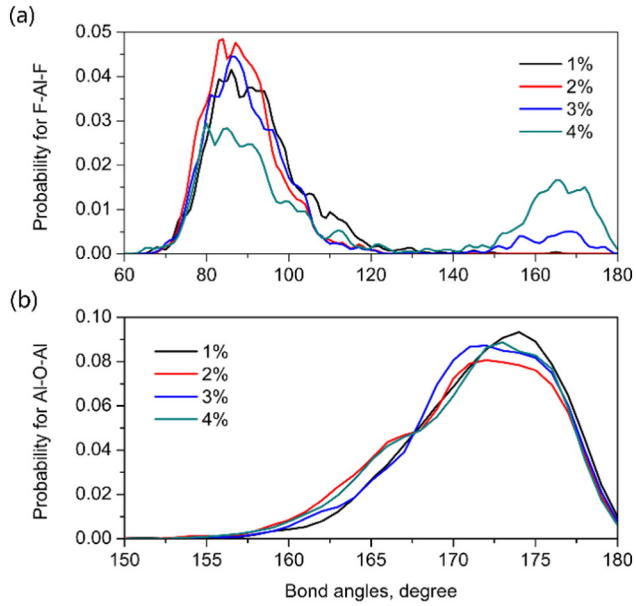

Fig. 3. Calculated probability distribution of bond angles (in degree) for F–Al–F (a) and Al–O–Al (b) of Na_3AlF_6–Al_2O_3 molten salt.

act as bridges connecting two Al^{3+} cations and arousing the partial polymerization of molten salt structure of Na_3AlF_6–Al_2O_3. In Na_3AlF_6–Al_2O_3 molten salt, the percentage of bridge F atom is small about 0.1–0.3%, not enough to determine the fluidity of molten salts, nevertheless these bridge O_b atoms can worsen the fluidity and transport properties.

3.2. Electronic structure

In Na_3AlF_6–Al_2O_3 molten salt, $[Al_2OF_6]^{2-}$ cluster is the key species according to our MD simulation. To insight the electronic structure properties such as density of states, electron density and Mulliken populations, the quantum chemical calculations for the selected $[Al_2OF_6]$ $[AlF_6]_3$ Na_{11} cluster from a certain MD trajectory were carried out. In a typical cluster of $[Al_2OF_6]$ $[AlF_6]_3$ Na_{11}, the central $[Al_2OF_6]^{2-}$ complex is surrounded by a second solvation shell with a total of three $[AlF_6]^{3-}$ and eleven Na^+ ions. Total and partial density of states (DOS) of a $[Al_2OF_6]$ $[AlF_6]_3$ Na_{11} cluster were obtained, as shown in Fig. 5. The electron orbitals near core with lowest energy around −50 eV were occupied by Na-3s states and electron orbitals with middle energy around −20 eV were occupied by Na-2p and F-2s states. In addition, the electron orbitals near the Fermi (HOMO) level is essentially dominated by O and F-2p states, with a hybridization with the Al-3s, 3p states. It indicates some covalent bond interactions (Al—F, Al—O) exist in the $[Al_2OF_6]^{2-}$ cluster and the possibility of electrons to transit from Al-3s, 3p to F-2p and O-2p states. Fig. 6 shows the electron density of a $[Al_2OF_6]$ $[AlF_6]_3$ Na_{11} cluster, the electrons transferring from the central

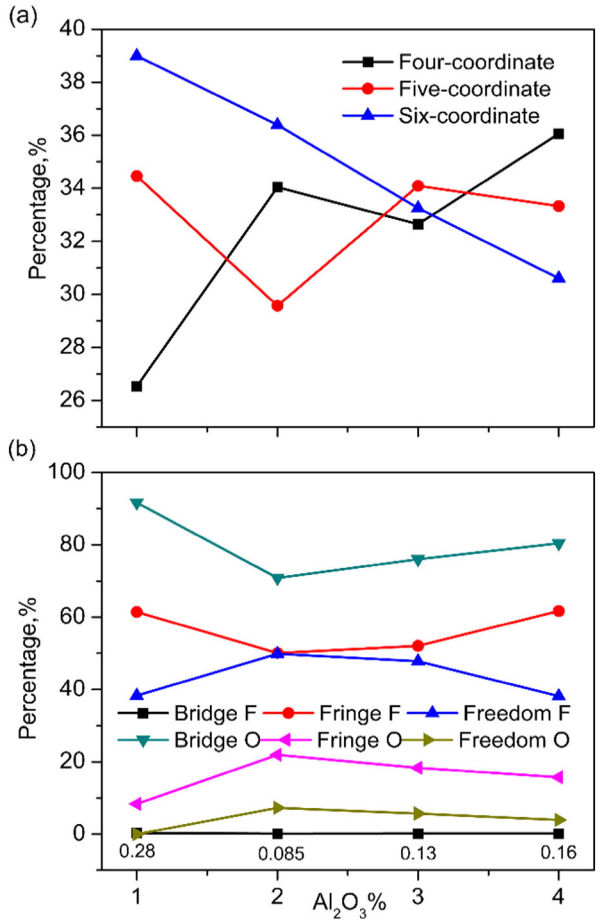

Fig. 4. Percentages of coordination numbers and F, O atom types of Na_3AlF_6–Al_2O_3 molten salt with 1–4 wt% Al_2O_3.

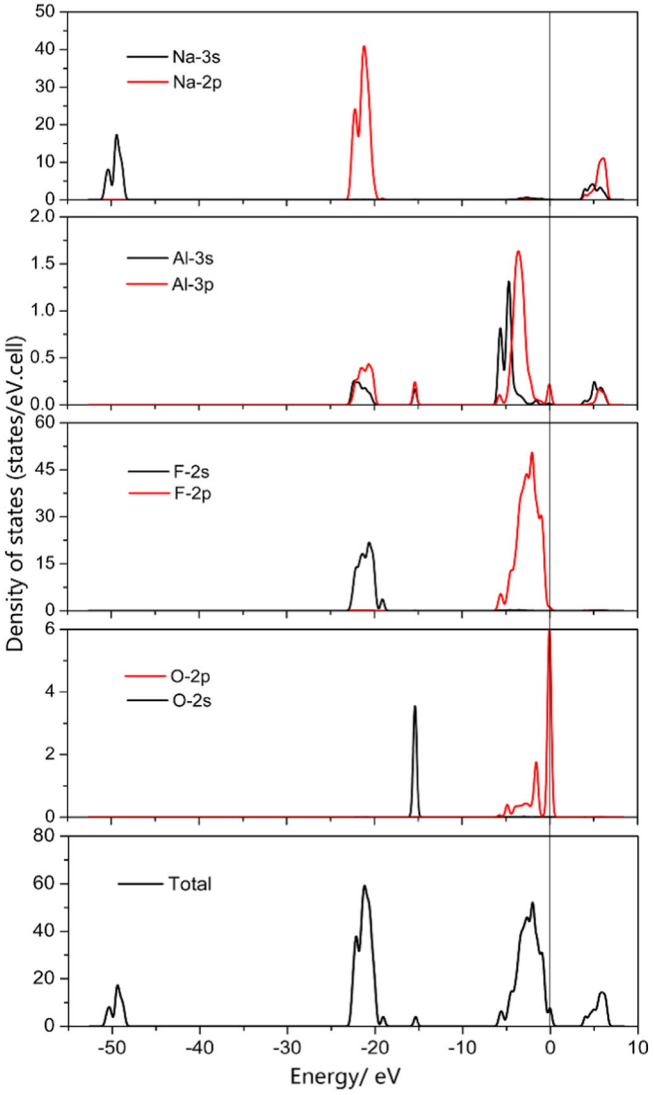

Fig. 5. Total and partial density of states (DOS) of a $[Al_2OF_6]$ $[AlF_6]_3$ Na_{11} cluster. The vertical gray line indicates the Fermi (HOMO) energy.

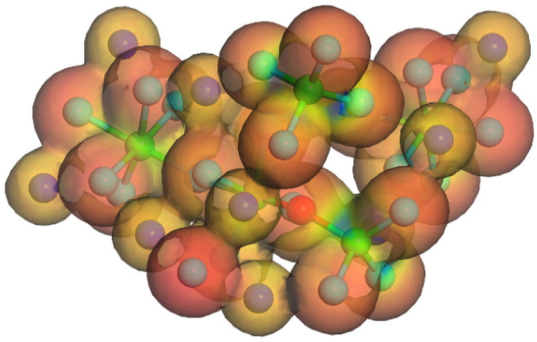

Fig. 6. Electron density of a $[Al_2OF_6]$ $[AlF_6]_3$ Na_{11} cluster. Insert: The central $[Al_2OF_6]^{2-}$ ion cluster.

Al atoms and surrounding Na atoms are mainly localized at F and O atoms, implying the distinct Coulomb interactions exist in the $[Al_2OF_6]$ $[AlF_6]_3$ Na_{11} cluster. Averaged Mulliken populations of the $[Al_2OF_6]$ $[AlF_6]_3$ Na_{11} cluster are listed in Table 5. The bond population of Al—O and Al—F is 0.53, 0.27, respectively, which is greater than the value of 0.035 of Na—F bond, implying the covalent character of formers are more evident than the latter. It is characteristic for Al—O and Al—F bonds are ionic as well as partial covalent due to the hybridization of O, F-2p and Al-3s (3p) orbitals, while the Na—F and F—F bonds are mainly ionic. These are in agreement with the results of above density of states (DOS) analysis.

3.3. Transport properties

Based on the computational methods in Section 2.5, the self-diffusion coefficients of all Na^+, Al^{3+}, F^- and O^{2-} ions in Na_3AlF_6–Al_2O_3 molten salt with 1–4 wt% Al_2O_3 were calculated, as shown in Fig. 7a. It can be noticed that the order of ion diffusion ability was found to be $Na^+ > F^- > Al^{3+} > O^{2-}$. The movement ability of ions is not only effected by the ionic radius, but also depends on the surrounding atomic interactions. Na^+ ions have smaller radius and are free, only for electrostatic interactions with surrounding particles, while Al^{3+}, F^- and O^{2-} ions exist in the form of $[AlF_x]^{3-x}$ and $[Al_2OF_6]^{2-}$, which have larger volume and resistance to motion. Al_2O_3 concentration has a significant impact on the diffusion ability. Adding more Al_2O_3 can increase the polymerization degree of the local structure in Na_3AlF_6–Al_2O_3 molten salt, all ions' self-diffusion coefficients reduce as a consequence. In addition, Na^+ and F^- are strongly affected by the change of Al_2O_3 concentration, while Al^{3+} and O^{2-} may not, it may be because of their own lower diffusion coefficients with smaller ranges for variation.

Then viscosity η was obtained (Fig. 7b) by combining the self-diffusion coefficient D and Einstein-Stokes approximation, and the step length λ of particle diffusion was considered to be equal to the diameter of Na ion, Al atom, F ion and O atom (λ = 2.04, 1.96, 2.66 and 3.04 Å). Al_2O_3 concentration has a strong impact on the viscosity of Na_3AlF_6–Al_2O_3 molten salt, the system's viscosity varies from 1.62 to 2.1 mP s with 1–4 wt% Al_2O_3. With the increase of Al_2O_3 percentage, the system's viscosity increases accordingly, it may be due to these larger volume groups $[Al_2OF_6]^{2-}$ worsening the liquidity of Na_3AlF_6–Al_2O_3 molten salt. Compared to the experimental value of 2.35 mP s [32] with 4 wt% Al_2O_3 in Na_3AlF_6–Al_2O_3 molten salt, our calculated result 2.18 mP s is in good agreement with it.

Table 5
Average Mulliken atomic orbital populations (s, p), total population (Total), charges transferred (Charge) and overlap population of $[Al_2OF_6]$ $[AlF_6]_3$ Na_{11} Cluster (unit: e).

Atoms	s	p	Total	Charges	Bonds	Population
Na	2.12	6.04	8.16	0.84	Na–F	0.035
Al	0.46	0.76	1.21	1.79	Al–F	0.27
F	1.96	5.76	7.72	−0.72	F–F	−0.03
O	1.86	5.38	7.24	−1.24	Al–O	0.53

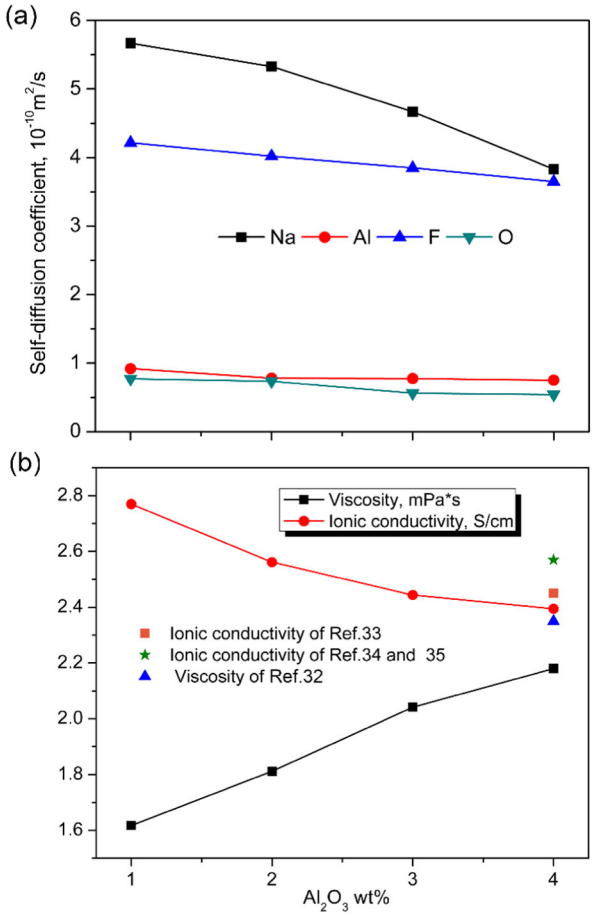

Fig. 7. Ions self-diffusion coefficient (a), viscosity and electric conductivity (b) of Na_3AlF_6–Al_2O_3 molten salt with 1–4 wt% Al_2O_3 compared with the experimental values of Ref.

Ionic conductivity σ was calculated by self-diffusion coefficient D of all Na^+, Al^{3+}, F^- and O^{2-} ions and Nernst-Einstein approximation, as presented in Fig. 7b. Ionic conductivity of molten salt also decreases dramatically from 2.77 to 2.39 S/cm with the increase of Al_2O_3 percentage. Combining above analysis of ion structure and viscosity, it is due to O atoms of Al_2O_3 play roles as bridges connecting the ionic structure networks and increase the polymerization degree of Na_3AlF_6–Al_2O_3 molten salt. The diffusion resistance of main charge carrier Na^+ and F^- increases, the ionic conductivity σ decreases as a consequence. Viewed from Fig. 7b, our calculated result of 2.39 S/cm is close to the experimental value 2.45 S/cm [33], 2.57 S/cm [34,35] of Na_3AlF_6–Al_2O_3 molten salt with 4 wt% Al_2O_3. It is noteworthy that the experimental data for Na_3AlF_6–Al_2O_3 molten salt is quite rare and the difficulty of experimental measurements under high temperature and strong corrosive environment may cause a certain errors of viscosity and ionic conductivity data.

On the other hand, the deviation of viscosity between calculated and experimental results implies that the MD simulation of transport properties are fastidious about the potential parameters. The computational accuracy and efficiency is a pair of contradictory for classical MD simulation. Therefore, ab initio molecular dynamics (AIMD) simulation of Na_3AlF_6–Al_2O_3 molten salt in the future work will be carried out, which is flexible to study any system without needing to firstly fit potential parameters to experimental or computed values. In view of our calculated lattice parameters of NaF, AlF_3, Na_3AlF_6 and Al_2O_3 crystals and ionic conductivity of Na_3AlF_6–Al_2O_3 molten salt with 4 wt% Al_2O_3 are in good agreement with experimental value, the conclusion can be

made that our MD simulation for structure and transport properties of Na_3AlF_6-Al_2O_3 molten salt are reasonable and reliable. In sum, the Al_2O_3 concentration has significant impact on the characters of both local structure and transport.

4. Conclusion

MD simulations with the Coulomb–Buckingham potential model were carried out to enhance the knowledge of local structure and transport properties of Na_3AlF_6–Al_2O_3 molten salt. The effect of Al_2O_3 concentration on basic structure-transport properties were calculated and compared to the experimental results to verify our MD simulation Na_3AlF_6–Al_2O_3 molten salt.

The $[AlF_4]^-$, $[AlF_5]^{2-}$ and $[AlF_6]^{3-}$ groups coexist in the Na_3AlF_6–Al_2O_3 molten salt and $[AlF_6]^{3-}$ ions are the dominant species at low concentration Al_2O_3 of 1–2 wt%, corresponding to the octahedral symmetries. Some $[AlF_4]^-$ and $[AlF_5]^{2-}$ ions can dissociate from $[AlF_6]^{3-}$ groups at higher concentration of Al_2O_3. The percentages of $[AlF_4]^-$, $[AlF_5]^{2-}$ and $[AlF_6]^{3-}$ groups are approximately equal at 3 wt% Al_2O_3 and $[AlF_4]^-$ ions become the major species at 4 wt% Al_2O_3. The O atoms mainly exist in the form of bridge O_b up to 90%, followed by non-bridge O_{nb}, suggesting most O^{2-} anions act as bridges connecting two Al^{3+} cations and worsening the fluidity and transport properties of molten salt. In Na_3AlF_6–Al_2O_3 molten salt, the percentage of bridge F atom is small about 0.1–0.3%, not enough to determine the fluidity, while these bridge O atoms can worsen the fluidity and transport properties.

According to quantum chemical calculations, Al—F and Al—O bonds in $[Al_2OF_6]^{2-}$ groups of Na_3AlF_6–Al_2O_3 molten salt have ionic characters as well as partial covalent characters due to the hybridization of F, O-2p and Al-3s (3p) orbitals, while the Na—F and F—F bonds are ionic. In addition, the order of ion diffusion ability follows as $Na^+ > F^- > Al^{3+} > O^{2-}$. Al_2O_3 play roles as bridges connecting the ionic structure networks and can increase the polymerization degree of the local structure in Na_3AlF_6–Al_2O_3 molten salt, the viscosity increases and ionic conductivity reduces accordingly. Our calculated results of ionic conductivity of Na_3AlF_6–Al_2O_3 molten salt with 4 wt% Al_2O_3 are in good agreement with the experimental results. In sum, the Al_2O_3 concentration has significant impact on both local structure and transport.

Acknowledgments

We sincerely acknowledge the High Performance Computing Center of CSU, China. This work was financially supported by the National Science and Technology Support Project of China (No.2012BAE08B02) and National Natural Science Foundation of China (No.51264011).

References

[1] W.B. J, JOM 51 (1999) 24.
[2] J.W. E, JOM 59 (2007) 30.
[3] H.K. James, W E, JOM 60 (2008) 25.
[4] R.R. Nazmutdinov, T.T. Zinkicheva, S.Y. Vassiliev, D.V. Glukhov, G.A. Tsirlina, M. Probst, Spectrochim. Acta A Mol. Biomol. Spectrosc. 75 (2010) 1244–1252.
[5] R.R. Nazmutdinov, T.T. Zinkicheva, S.Y. Vassiliev, D.V. Glukhov, G.A. Tsirlina, M. Probst, Chem. Phys. 412 (2013) 22–29.
[6] S. Cikit, Z. Akdeniz, P.A. Madden, J. Phys. Chem. B 118 (2014) 1064–1070.
[7] X. Lv, Z. Xu, J. Li, J. Chen, Q. Liu, J. Fluor. Chem. 185 (2016) 42–47.
[8] V.L.E. Robert, C. Bessada, D. Massiot, B. Gilbert, J.-P. Coutures, Inorg. Chem. 38 (1999) 214–217.
[9] B.M. Gilbert, T, Appl. Spectrosc. 44 (1990) 299–305.
[10] B.R. Gilbert, E. Tixhon, J. Olsen, T. Ostvold, Inorg. Chem. 35 (1996) 4198–4210.
[11] P.A.M. Zehra, Akdeniz, J. Phys. Chem. B 110 (2006) 6683–6691.
[12] W.J. Glover, P.A. Madden, J. Chem. Phys. 121 (2004) 7293.
[13] C.B. Vincent Lacassagne, P. Florian, S. Bouvet, B. Ollivier, J.-P. Coutures, D. Massiot, J. Phys. Chem. B 106 (2002) 1862–1868.
[14] O.I.O.D.K. Belashchenko, S.Y.U. Saposznikova, Metall. Mater. Trans. B 29B (1998) 105–110.
[15] I.F. Jonathan, F. Stebbins, N. Dando, S.-Y. Tzeng, J. Am. Ceram. Soc. 75 (1992) 3001–3006.
[16] V.L.C. Bessada, D. Massiot, P. Florian, J.-P. Coutures, E. Robert, B. Gilbert, Z. Naturforsch. A 54 (1999) 162–166.
[17] A. Bengtson, H.O. Nam, S. Saha, R. Sakidja, D. Morgan, Comput. Mater. Sci. 83 (2014) 362–370.
[18] X. Lv, Z. Xu, J. Li, J. Chen, Q. Liu, J. Mol. Struct. 1117 (2016) 105–112.
[19] G. Malavasi, A. Pedone, M.C. Menziani, J. Phys. Chem. B 117 (2013) 4142–4150.
[20] T. Wu, S. He, Y. Liang, Q. Wang, J. Non-Cryst. Solids 411 (2015) 145–151.
[21] P. Zhang, W. Hui, Y. Zhang, X. Ren, D. Zhang, J. Non-Cryst. Solids 358 (2012) 1465–1473.
[22] E. Gambuzzi, A. Pedone, Phys. Chem. Chem. Phys. 16 (2014) 21645–21656.
[23] T. Kitamura, Y. Umeno, F. Shang, T. Shimada, K. Wakahara, J. Solid Mech. Mater. Eng. 1 (2007) 1423–1431.
[24] B.J.K.Q. Zhou, J. Solid State Chem. 177 (2004) 654–659.
[25] C.R.A.C.J.D. Galet, W.C. Mackrodt, Model. Simul. Mater. Sci. Eng. 1 (1992) 73–81.
[26] N. de Koker, Geochim. Cosmochim. Acta 74 (2010) 5657–5671.
[27] F.J. Spera, M.S. Ghiorso, D. Nevins, Geochim. Cosmochim. Acta 75 (2011) 1272–1296.
[28] F.J. Spera, D. Nevins, M. Ghiorso, I. Cutler, Geochim. Cosmochim. Acta 73 (2009) 6918–6936.
[29] J.M. Ziman, Principles of the Theory of Solids, Cambridge University Press, Cambridge University, 1972.
[30] R. Kubo, Rep. Prog. Phys. 29 (1966) 255–284.
[31] C.C. Miller, Proc. R. Soc. Lond. A 106 (1924) 724–749.
[32] R.P.T.T.G.J. Janz, J. Phys. Chem. Ref. Data 5 (1983) 591–815.
[33] E.W.Y.a.M. Feinleib, J. Electrochem. Soc. 104 (1957) 626–630.
[34] C.S.T.J.S. Edwards, L.A. Cosgrove, A.S. Russel, J. Electrochem. Soc. 100 (1953) 508–512.
[35] O.K.P. Fellner, A. Sterten, J. Thonstad, Electrochim. Acta 38 (1993) 589–592.